Precisely Mapping the Absolute Magnetic Field in Vacuum by an Optical Ramsey Atom Interferometer

Xiao-Bing Deng, Yao-Yao Xu, Xiao-Chun Duan,* and Zhong-Kun Hu†
MOE Key Laboratory of Fundamental Quantities Measurement, Hubei Key Laboratory of Gravitation and Quantum Physics, School of Physics, Huazhong University of Science and Technology, Wuhan 430074, China

(Received 13 July 2020; revised 25 March 2021; accepted 7 May 2021; published 27 May 2021)

Atoms in magnetically sensitive sublevels constitute a natural sensor for absolute magnetic field measurements, which are explored here to form an optical Ramsey interferometer for determining the magnetic field distribution. An optical Ramsey atom interferometer provides a convenient way to map a magnetic field in vacuum. In comparison with the often used Raman spectroscopy method, a Ramsey interferometer can not only improve the sensitivity, but also dramatically suppress the contribution of the ac Stark effect. Furthermore, in this work, the magnetically sensitive atoms are velocity-selected, which improves the spatial resolution for the magnetometer as well as the contrast of the Ramsey fringes. A short-term sensitivity of 1.4 nT/Hz$^{1/2}$ for magnetic field measurement is finally achieved even with an interrogation time as short as 500 μs. The presented approach for absolute magnetic field measurement is expected to find wide applications in atom-interferometry-based precision measurements.

DOI: 10.1103/PhysRevApplied.15.054062

I. INTRODUCTION

In the last three decades, atom interferometry techniques have been rapidly developed and found many important applications, spanning from inertial sensors [1–6] and atomic clocks [7–9] to fundamental physical quantity measurement [10,11], tests of fundamental laws of physics [12–17], and probing short-range forces [18–20]. In many of these applications, knowledge of the magnetic field experienced by atoms has to be acquired precisely to estimate the corresponding influence [21]. A magnetic field can be measured by many methods, such as the superconducting quantum interference device (SQUID) method with a sensitivity of 1 fT/Hz$^{1/2}$ [22], the spin-exchange relaxation-free (SERF) method with an ultrahigh sensitivity of 0.16 fT/Hz$^{1/2}$ [23], the nonlinear magneto-optical rotation (NMOR) method with a sensitivity of 1 fT/Hz$^{1/2}$ [24,25], and the coherent population trapping (CPT) method with a sensitivity of 8 pT/Hz$^{1/2}$ [26]. Although these methods have ultrahigh sensitivity for magnetic field measurement, they are not handy for the above mentioned atom-interferometry-based applications, either owing to their respective limited dynamic range and/or operation conditions or because they cannot achieve a perfectly collocated measurement with respect to the atomic trajectories inside a vacuum chamber. In this work, we investigate the potential of magnetically sensitive optical Ramsey interferometry for resolving an absolute magnetic field in a vacuum chamber.

As an ingenious method of separated oscillatory fields [27], Ramsey interferometry has been widely used in physics experiments, particularly in the field of atomic clocks [28]. Although it is well known for measuring the absolute frequency of an atomic transition, there are only a few reports in the literature in which Ramsey interferometry is explored to measure a magnetic field using magnetically sensitive transitions [29–39], not even to say optical Ramsey interferometry. Instead, spectroscopy using a single oscillatory field, either stimulated Raman transitions [21,40–42] or microwave transitions [42,43], is usually adopted. In Ref. [37], a magnetometer is realized using a single electronic spin in diamond by Ramsey interferometry, with a sensitivity of about 500 nT/Hz$^{1/2}$. In Ref. [32], Ramsey interferometry, comprising two magnetically sensitive microwave transitions, is explored to measure the time-averaged magnetic field over long flight times. And the magnetic field profile has to be deconstructed from many measured time-averaged values at different fountain heights, which increases the complexity and usually results in a poor spatial resolution for magnetic field mapping.

In this work, magnetically sensitive Ramsey interferometry based on stimulated Raman transitions is explored to measure the magnetic field in an atomic fountain. Compared with spectroscopy involving a single oscillatory field, the Ramsey interferometry method can improve the sensitivity as a consequence of increased interrogation

*duanxiaochun2011@hust.edu.cn
†zkhu@hust.edu.cn

time. In addition, compared with Raman spectroscopy, the ac Stark shift is absent during the free evolution period for an optical Ramsey interferometer, which means that the ac Stark effect will be greatly suppressed. And in comparison with microwave-transition-based Ramsey interferometry as well as other magnetometers, like those based on the SQUID, SERF, NMOR, and CPT methods, Ramsey interferometry based on stimulated Raman transitions is much more convenient for mapping the magnetic field distribution of a certain zone, especially inside a vacuum chamber serving as an atom interferometry sensor where other magnetic detection sensors cannot readily access.

Usually, a magnetic field is probed by atoms without velocity selection, where the atomic cloud expands fast. The measured magnetic field is actually an average of the field experienced by a large atom cloud, ending up with poor spatial resolution. In this work, besides preparing atoms in magnetically sensitive sublevels, atoms are also velocity selected in the vertical direction using a Raman π pulse in Doppler-sensitive configuration before encountering the magnetic field measurement sequence. In this way, the spatial resolution can be improved by about 5 times, achieving about 1 mm in our experiment. Finally, a short-term sensitivity of 1.4 nT/Hz$^{1/2}$ for absolute magnetic field measurement is demonstrated here even with a short interrogation time of 500 μs.

II. THEORETICAL ANALYSIS

Ramsey spectroscopy usually takes an atomic clock transition line as a frequency reference. For magnetic field measurement, the Zeeman effect is explored to sense the magnitude of the magnetic field, as shown in Fig. 1(b). With ^{87}Rb atoms prepared in a magnetically sensitive sublevel $|m_F\rangle$ ($m_F = +1$ or -1) of the hyperfine state $|F = 1\rangle$, when subjected to a $\pi/2 - \pi/2$ Doppler-insensitive Raman pulse sequence, atoms will oscillate between $|F = 1, m_F\rangle$ and $|F = 2, m_F\rangle$, manifesting a magnetically sensitive Ramsey fringe. The transition probability can be expressed as

$$P = A - \frac{C}{2}\cos(\Delta\phi), \tag{1}$$

where A and C stand for the fringe offset and contrast, respectively. The total phase shift is

$$\Delta\phi = (\delta - \delta_B)T\left(1 + \frac{4\tau}{\pi T}\right) - \frac{4}{\pi}\delta_{\mathrm{AC}}\tau, \tag{2}$$

where τ is the duration of the $\pi/2$ pulse and T is the interrogation time between the two $\pi/2$ pulses. The effect of Raman pulse duration must be taken into consideration since the interrogation time is typically quite short in a magnetically sensitive interferometer. $\delta = \omega_L - \omega_0$

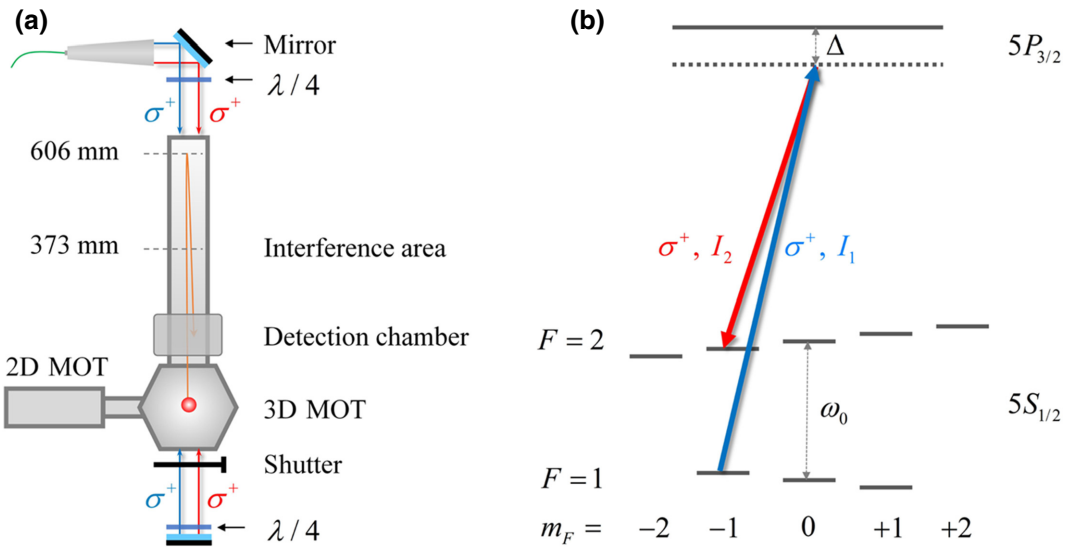

FIG. 1. (a) Schematic of the vacuum cell and polarization configuration of Raman beams in the vacuum chamber, as well as (b) energy level scheme of magnetically sensitive Raman transition for ^{87}Rb. A mechanical shutter is integrated to switch between Doppler-sensitive and Doppler-insensitive Raman laser configurations. When applying two phase-locked laser beams with a polarization combination of $\sigma^+\sigma^+$ or $\sigma^-\sigma^-$, atoms will undergo a stimulated Raman transition between $|F = 1, m_F\rangle$ and $|F = 2, m_F\rangle$. For simplicity, here only the $\sigma^+\sigma^+$ transition and the case of $|m_F = -1\rangle$ are displayed. The transition between $|F = 1, m_F = +1\rangle$ and $|F = 2, m_F = +1\rangle$ could be combined to perform a differential measurement. I_1 and I_2 are the corresponding densities for the two beams.

represents the detuning of the Raman laser effective frequency ω_L with respect to the ^{87}Rb atom clock transition line ω_0. δ_B is the Zeeman shift, namely the differential energy shift between $|F=1,m_F\rangle$ and $|F=2,m_F\rangle$ induced by the magnetic field. For the first-order Zeeman shift, $\delta_B = 2\alpha_{Z,I} m_F B$, where $\alpha_{Z,I} = 2\pi \times 0.7$ MHz/G is the first-order Zeeman coefficient of ^{87}Rb atoms in $5^2\mathbf{S}_{1/2}$ electronic state and B is the magnetic flux density experienced by the atoms. The effect of differential ac Stark shift $\delta_{\rm ac}$, which only occurs during the Raman pulses, is also included in $\Delta\phi$.

Ramsey fringes are obtained by sweeping the effective frequency ω_L of Raman lasers, which modulates the detuning δ. The central fringe corresponding to zero detuning could be determined by examining the superposition of fringes with different interrogation time T. In our situation, an appropriate value of δ, denoted as δ_0, can be found around the fringe center to make $\Delta\phi = 0$. Thus the magnetic field can be determined as

$$B_{m_F} = \frac{1}{2\alpha_{Z,I} m_F}\left[\delta_0 - \frac{4\tau}{\pi T + 4\tau}\delta_{\rm ac}\right]. \tag{3}$$

We notice that both δ_0 and $\delta_{\rm ac}$ are dependent on the value of m_F. In order to improve the measurement precision, Ramsey interferometers with $|m_F=+1\rangle$ and $|m_F=-1\rangle$ are combined to make a differential measurement, and the magnetic field can be deduced as

$$B = \frac{1}{2\alpha_{Z,I}}\left[\frac{\delta_0^{+1} - \delta_0^{-1}}{2} - \frac{4\tau}{\pi T + 4\tau}\frac{\delta_{\rm ac}^{+1} - \delta_{\rm ac}^{-1}}{2}\right], \tag{4}$$

where the superscript $+1$ and -1 stand for $|m_F=+1\rangle$ and $|m_F=-1\rangle$, respectively.

To measure the magnetic field accurately, the influence of ac Stark shift must be evaluated. In Doppler-insensitive Raman transitions, Raman lasers are usually configured with a polarization combination of $\sigma^+\sigma^+$ or $\sigma^-\sigma^-$. Taking $\sigma^+\sigma^+$ as an example, the ac Stark shift for different sublevels can be expressed as

$$\delta_{\rm ac}^i = \kappa[\alpha^i I_1 - \beta^i I_2], \tag{5}$$

where the superscript $i = +1, 0, -1$ denotes that the atoms are in $|m_F=+1,0,-1\rangle$, respectively. κ is a constant related to the transition dipole matrix elements of the ^{87}Rb D_2 transition line. I_1 and I_2 are the intensities of the two Raman beams, as shown in Fig. 1(b). α^i and β^i are the coupling coefficients, which are determined by the detunings for single-photon transitions and dipole matrix elements. They are calculated as [21,44,45]

$$\alpha^{+1} = \frac{5}{12(\Delta+\omega_0)} - \frac{1}{4\Delta}, \quad \beta^{+1} = \frac{1}{4(\Delta-\omega_0)} - \frac{5}{12\Delta}, \tag{6}$$

$$\alpha^{-1} = \frac{1}{4(\Delta+\omega_0)} - \frac{5}{12\Delta}, \quad \beta^{-1} = \frac{5}{12(\Delta-\omega_0)} - \frac{1}{4\Delta}, \tag{7}$$

and

$$\alpha^{0} = \frac{1}{3(\Delta+\omega_0)} - \frac{1}{3\Delta}, \quad \beta^{0} = \frac{1}{3(\Delta-\omega_0)} - \frac{1}{3\Delta}. \tag{8}$$

According to the expressions, we can deduce that

$$\alpha^0 = \frac{\alpha^{+1} + \alpha^{-1}}{2}, \quad \beta^0 = \frac{\beta^{+1} + \beta^{-1}}{2}, \tag{9}$$

resulting in

$$\delta_{\rm ac}^0 = \frac{\delta_{\rm ac}^{+1} + \delta_{\rm ac}^{-1}}{2}, \tag{10}$$

where Δ denotes the far detuning for two-photon Raman transitions, which is around 1.5 GHz in our experiment. In the expressions of α^i and β^i, the hyperfine splittings of the excited state $5^2\mathbf{P}_{3/2}$ are ignored. With the hyperfine splittings considered, the expressions of α^i and β^i will vary slightly. But the relations in Eqs. (9) and (10) are still approximately satisfied. According to Eqs. (6) and (7), it is impossible to ensure $\delta_{\rm ac}^{+1} = \delta_{\rm ac}^{-1} \equiv 0$ at the same time for directly canceling ac Stark shift by adjusting the intensity ratio I_1/I_2. Generally, one can readily adjust the intensity ratio to make sure $\delta_{\rm ac}^0 = 0$ prior to knowing the first-order Zeeman shift because there is only a second-order Zeeman shift when atoms are in $|m_F=0\rangle$ [46]. In this case, it can be deduced that $\delta_{\rm ac}^{+1} + \delta_{\rm ac}^{-1} \approx 0$, namely equal amplitude but opposite signs. We note that in the Raman spectroscopy method, the influence of ac Stark shift cannot be eliminated by differential measurement using opposite magnetic sublevels either. But in comparison, the influence of the ac Stark shift can be suppressed by a factor of $(\pi T + 4\tau)/4\tau$ in our Ramsey method here.

III. MAGNETIC FIELD MEASUREMENT

A. Experimental setup and procedure

The proof-of-principle experiment is performed using one of our interferometers reported previously [47,48]. A schematic of our vacuum chamber is shown in Fig. 1(a). One cycle starts by loading ^{87}Rb atomic cloud in the three-dimensional magneto-optical trap (3D MOT), which is fed by a two-dimensional MOT. After a loading time of 315 ms, about 10^8 atoms are launched upward with an initial velocity of 3.44 m/s by a far-detuned optical moving

molasses, during which the atoms are further cooled to a temperature of 6 μK through polarization gradient cooling. This temperature corresponds to a velocity distribution width of $\sigma_v = 23.4$ mm/s. Repumping light for the 3D MOT is turned off later than the six trapping beams so that all the atoms end up in $|F = 2\rangle$ hyperfine ground state in the atom fountain. After entering the interference area, atoms are firstly state-prepared before being subjecting to the interferometry sequence. A solenoid coil is tightly wrapped on the outer cylinder of the interference tube to provide a quantization axis for removing the degeneracy of the sublevels in hyperfine states. And a five-layer μ-metal film is added immediately outside of the coil for shielding stray magnetic field.

In common Doppler-insensitive atom interferometers, it is usual to select atoms in a certain internal state, but without velocity selection. In this work, in order to improve the spatial resolution for magnetic field measurement, both internal state and velocity selection are performed. A counter-propagating (Doppler-sensitive) Raman π pulse is utilized to implement the required state preparation.

The Raman lasers are originated from two external cavity diode lasers (Toptica DL pro). Before injecting into the same tapered amplifier (TA), they are superposed and phase locked with an optical phase-locking loop (OPLL). The output beams from the TA pass through an acousto-optical modulator operating at 1.5 GHz. And the negative first-order diffraction beams are used for the Raman lasers, which are thus largely detuned for avoiding spontaneous emission. The beams are guided to a collimator located on the top of the vacuum system through a polarization-maintaining fiber. A first quarter-wave plate (QWP), which is installed over the top of the interference tube, realizes circular polarization. At the bottom, there is a mirror for retro-reflecting the two Raman beams to form the counter-propagation configuration for Doppler-sensitive Raman transitions during state preparation. There is a second QWP immediately over the mirror to ensure correct polarization for reflected Raman lasers. A mechanical shutter is installed over the second QWP to block the retro-reflected Raman lasers during the interfering process, which ensures Doppler-insensitive Raman transitions for interfering. The time for completely opening or closing the shutter is about 30 ms. This time is short enough for switching between the two configurations of the Raman lasers. It is also worth noting that the effective frequencies of the Raman lasers are completely different for the two configurations due to Doppler detuning. And the hop of the frequency between the two configurations is realized by the frequency shift key feature of an arbitrary function generator used as frequency reference in the OPLL for the Raman lasers. Unwanted atoms left in $|F = 2\rangle$ are blown away with a beam tuned to resonance on $|F = 2\rangle$ to $|F' = 3\rangle$ of $5^2\mathbf{P}_{3/2}$. This state preparation selects out about 10^6 atoms in required $|F = 1, m_F\rangle$, and reduces the vertical velocity spread of the cloud down to about 3.8 mm/s. The selected atoms are then subjected to a $\pi/2 - \pi/2$ Doppler-insensitive Raman pulse sequence. The duration of each Raman $\pi/2$ pulse is 20 μs. The interrogation time is set as 500 μs, which ensures a relatively high contrast for the Ramsey fringe and also a good spatial resolution for magnetic field measurement. In the end, normalized time-of-flight (TOF) fluorescence detection is performed to deduce the transition probability when atoms fall back into the detection zone. The whole procedure described above composes one shot for magnetic field measurement, and it takes 1 s.

The Ramsey fringes are obtained by modulating the effective frequency of the Raman lasers from shot to shot, and typical fringes are shown in Fig. 2. At a specific point in space, the fringe center can be located by examining the superposition of fringes for different T. Normally, the

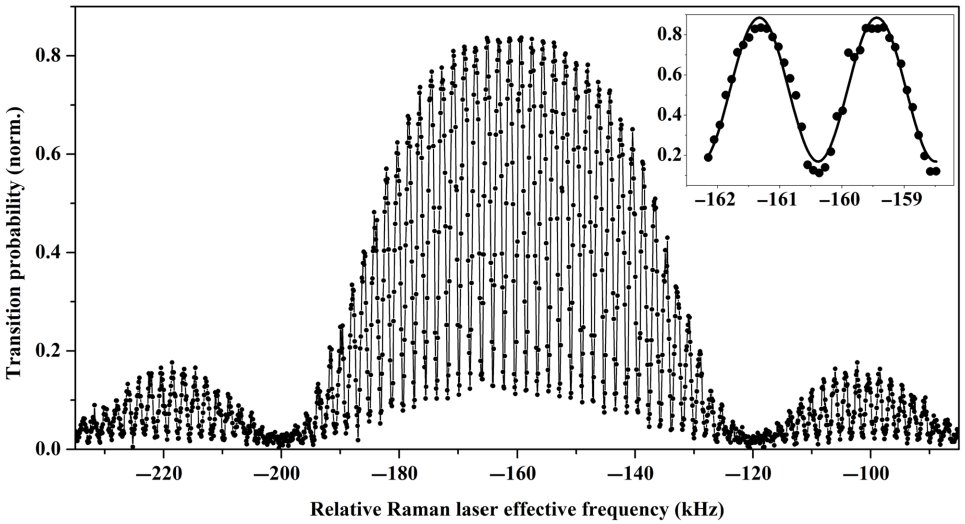

FIG. 2. Typical Ramsey fringes for the magnetically sensitive interferometer. Atoms are prepared in $|F = 1, m_F = -1\rangle$ in the preparation stage, and the Raman transition occurs between $|F = 1, m_F = -1\rangle$ and $|F = 2, m_F = -1\rangle$. The free evolution time is $T = 500$ μs. The solid line is plotted as a guide to the eye. Inset: enlargement of the central fringe.

fringe center search is necessary at only one point in space since the magnetic field does not vary much from point to point in our case.

B. ac-Stark shift measurement

To derive the magnetic field accurately, it is a prerequisite to evaluate the ac Stark shift. We also explore Ramsey interferometry to measure the ac Stark shift [1]. During the free evolution time of Ramsey interferometry, a Raman pulse with a changeable duration is inserted to induce an additional phase shift, which is proportional to the ac Stark shift and the pulse duration. This inserted Raman pulse must be detuned far enough from the resonance Raman transitions to avoid stimulating the atoms, but meanwhile small enough to keep the induced ac Stark shift as close as possible to the one to be measured. A detuning of 15 MHz is chosen here, which is realized by a radio-frequency switch to change the reference frequency source of the OPLL. Before measurement, the intensity ratio of the two Raman lasers is precisely adjusted to ensure $\delta_{\mathrm{ac}}^{0} \sim 0$ following the general procedure [46]. Results are shown in Fig. 3. As expected, the induced phase variation changes linearly with the duration of the inserted pulse for all three magnetic sublevels. The slopes correspond to their ac Stark shifts. The fitted slopes are $\delta_{\mathrm{ac}}^{+1} = +2\pi \times 3.44(7)$ kHz, $\delta_{\mathrm{ac}}^{-1} = -2\pi \times 3.50(7)$ kHz, and $\delta_{\mathrm{ac}}^{0} = +2\pi \times 0.06(13)$ kHz. These values agree well with the proposed relation in Eq. (10). The shifts of $\delta_{\mathrm{ac}}^{+1}$ and $\delta_{\mathrm{ac}}^{-1}$ are used to calculate the correction in the magnetic field measurement due to the ac Stark effect. The correction is as high as 248 nT for the Raman spectroscopy method, but is only 12 nT for the Ramsey method, which corresponds to a suppressed factor of over 20.

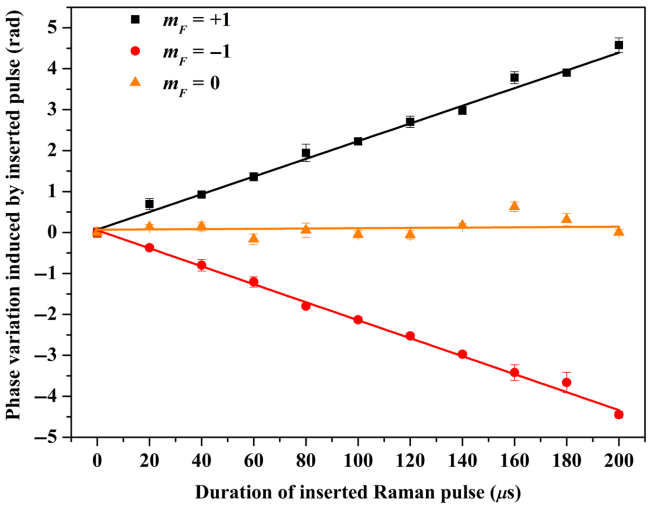

FIG. 3. Measurement of the ac Stark shift for different sublevels. The solid lines are the respective linear fittings. The slopes are the ac Stark shifts of corresponding magnetic sublevels. These measured results are used to calculate the corrections due to the ac Stark effect in the magnetic field measurement.

C. Mapping the magnetic field distribution

Measurements with atoms prepared in $|F = 1, m_F = -1\rangle$ and $|F = 1, m_F = +1\rangle$ are performed alternately. Two adjacent measurements from the two sublevels are combined to derive one determination of the absolute magnetic field. At one point in space, we repeat this differential measurement 10 times. The magnetic field within 373 to 606 mm is mapped by moving the interferometry sequence upward step by step with a time increment of 4 ms. This region is the typical interference area for our g measurement. The resulting magnetic field distribution along the central axis of our vacuum chamber is depicted in Fig. 4(a). The vertical error bars show the statistical error. For comparison, mapped magnetic field distributions using the Ramsey method without velocity selection and the Raman spectroscopy method are also displayed. The distributions for the three methods agree well with each other, which verifies the corrections of the ac Stark effect for the different methods. The discrepancy of abscissa values shown clearly in the inset of Fig. 4(a) comes from the velocity difference due to velocity selection. Comparing with Raman spectroscopy, the Ramsey method shows an obvious advantage of higher precision. And compared with the Ramsey method without velocity selection, velocity selection can improve the spatial resolution significantly, which is discussed in detail below.

The spatial resolution for magnetic field measurement here depends on the atomic cloud vertical size and the movement during interrogation. While it is convenient to map the magnetic field using a moving atomic cloud, the movement of atoms indeed deteriorates the spatial resolution. The total interrogation time is $2\tau = 40$ μs for the Raman spectroscopy method and $T + 2\tau = 540$ μs for the Ramsey method. Thus the atoms indeed move for a longer time in the Ramsey method during interrogation. However, for an interrogation time as short as 500 μs, this factor is not the primary limitation for the spatial resolution as we will show. Taking the midpoint (490 mm) as an example, the corresponding flight time after launch is about 198 ms and the velocity there is about 1.5 m/s. The moving distance is about 0.06 mm for the Raman spectroscopy method and about 0.8 mm for the Ramsey method. Taking half of the distance as the contribution to the spatial resolution, the corresponding values are 0.03 and 0.4 mm, respectively. However, due to spread, the vertical size of the atomic cloud without velocity selection becomes 4.7 mm when considering a typical value of 0.5 mm for the initial size. This means that the spatial resolutions for the Raman spectroscopy method and Ramsey method without velocity selection will be limited to be about 5 mm due to spread. Using vertical velocity

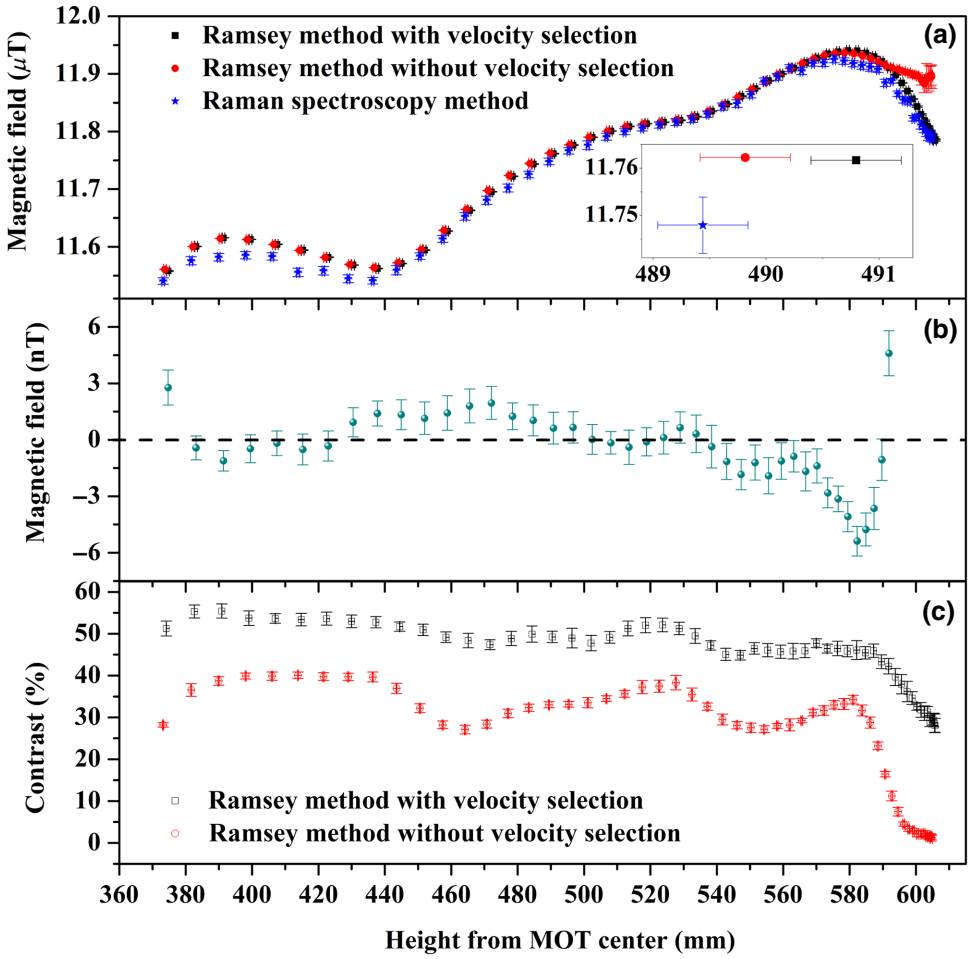

FIG. 4. (a) Magnetic field distributions measured by the Ramsey interferometer using atoms with (black squares) and without (red dots) velocity selection. For comparison, mapped magnetic field using the general Raman spectroscopy method is also depicted (blue stars). (b) The difference between measured magnetic field by the Ramsey method without and with velocity selection. (c) Corresponding variations of contrast. Magnetic field along the center axis of our vacuum chamber is mapped by changing the beginning time of the first $\pi/2$ pulse step by step. The time between neighboring measurements is 4 ms. Error bars are smaller than the size of the markers on the plot. Inset in (a): the plot of measurements around 490 mm is enlarged for seeing the error bars clearly.

selection, the spatial resolution can be improved to about 1 mm for the Ramsey method. The horizontal error bar in Fig. 4 accounts for the uncertainty of the center position of the atomic cloud, where the effect of fountain fluctuation dominates. The shot-to-shot position variation due to fountain fluctuation is measured as 0.4 mm, and thus the final horizontal error bar is 0.4 mm.

Since the size of the atomic cloud along the vertical direction is quite large without velocity selection, it is supposed that different parts of the cloud experience different magnetic field. Thus the measured value is actually an average over all the atoms in the atomic cloud. This average effect has two consequences. One is the inhibition of the precision. There is a local maximum of the magnetic field around 580 mm shown in Fig. 4(a). It can be imagined that the measurement result will deviate from the actual value due to the average effect when the center of the atomic cloud arrives at this point. And a wider atomic cloud gives a smaller measurement value. This is clearly shown around 580 mm in Fig. 4(b), which corresponds to the difference of the magnetic field measurements between Ramsey methods without and with velocity selection. The difference is greatest around 580 mm as expected. The other consequence is the degradation of the fringe contrast. The transition probabilities after the interfering pulses will not be the same for different parts of the atom cloud if the magnetic field is inhomogeneous over the cloud. The fringe corresponds to an average of the transition probabilities for all the atoms participating in the interference, and thus the fringe contrast will decrease for nonzero atomic cloud size. The contrast decreases more for a wider atomic cloud, which is clearly shown in Fig. 4(c). As predicted, the contrast for Ramsey fringes without velocity selection is at least 20% lower than that with velocity selection throughout the measurement region. In addition, it can be seen that both the contrasts decay rapidly when the magnetic field varies rapidly, for example, after the point of 580 mm, but the contrast for the fringes without velocity selection decays much faster than that with velocity selection.

It is also interesting to examine the TOF signal for the interferometer without velocity selection. As discussed above, the transition probabilities of atoms in different parts of the cloud will vary when encountering an inhomogeneous magnetic field, which may lead to multiple peaks in the TOF signal. This is indeed observed in the

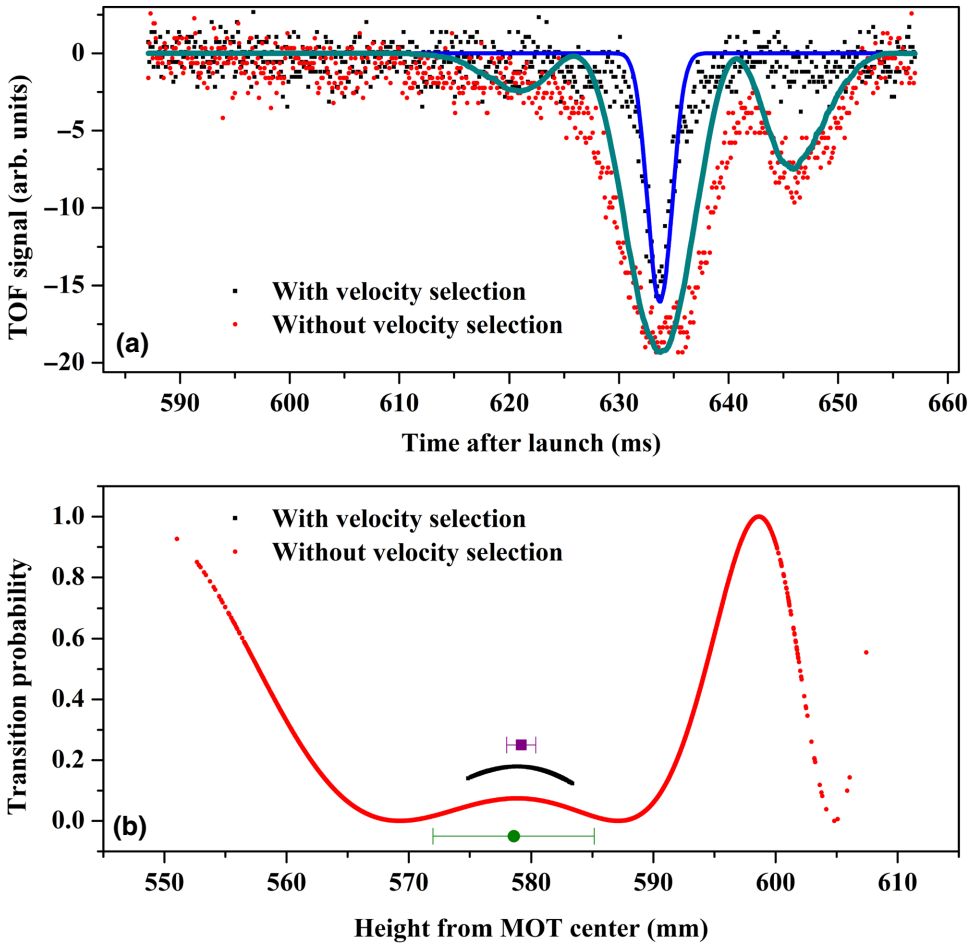

FIG. 5. (a) Measured (black squares and red dots) and simulated (blue and cyan solid lines) TOF profiles in the Ramsey method with and without velocity selection. The detected TOF signal is reversed due to a negative current-to-voltage conversion. (b) Corresponding transition probabilities of atoms in the simulation versus their position at 278 ms. The purple square and green dot indicate the centers of the clouds with and without velocity selection, respectively, and the error bars represent the corresponding cloud sizes.

experiment, as shown with red dots in Fig. 5(a). The TOF signal is obtained through fluorescence detection when atoms fall back into the detection chamber. It is proportional to the atoms transited to $|F = 2\rangle$ hyperfine states after the interference that takes place at the local maximum around 580 mm. The multiple-peak feature of the TOF signal is an intuitive representation of the view that atoms within the large cloud behave differently. A simulation is further carried out to directly manifest the different behaviors of the atoms during the interference, which is shown in Fig. 5(b) (red dots). In the simulation, a cloud with 10^5 atoms is generated. For each atom, an initial position and velocity are assigned from a list of numbers generated from Gaussian distributions, where only the vertical dimension is considered. The center of the position distribution corresponds to the initial cloud central position, which is set at the center of the 3D MOT, and the standard deviation of the position distribution corresponds to the cloud initial size, which is assigned a typical value of 0.5 mm. The center of the velocity distribution corresponds to the initial velocity of the cloud after launch (3.44 m/s), and the standard deviation of the velocity distribution corresponds to the velocity spread (23.4 mm/s). Each atom follows a ballistic trajectory after launch and the cloud spreads freely during the flight. After a flight time of 278 ms, atoms are subjected to the interference pulses, and the transition probability for each atom can be calculated. In the calculation, the magnetic field distribution mapped by the Ramsey method with velocity selection is used. As shown in Fig. 5(b), the transition probabilities of atoms indeed vary within the large cloud. The position distribution of the cloud after a flight time of 278 ms can also be obtained by counting the position of each atom. The center and standard deviation are depicted by the green dot and error bar, respectively. The standard deviation is 6.6 mm, corresponding to the cloud size. For comparison, the simulation is also carried out for the situation with velocity selection [black squares in Fig. 5(b)]. The procedure is the same except that the standard deviation for the initial velocity distribution is 3.8 mm/s accounting for velocity selection. Correspondingly, the center and the standard deviation of the position distribution for the atoms after a flight time of 278 ms are indicated by the purple square and error bar. The standard deviation implies that the cloud size is only 1.2 mm in this case. The simulated clouds continue flying freely for another 309 ms, arriving at the detection chamber, where the corresponding TOF signals can be calculated. The TOF signals depend on both the transition probability and the

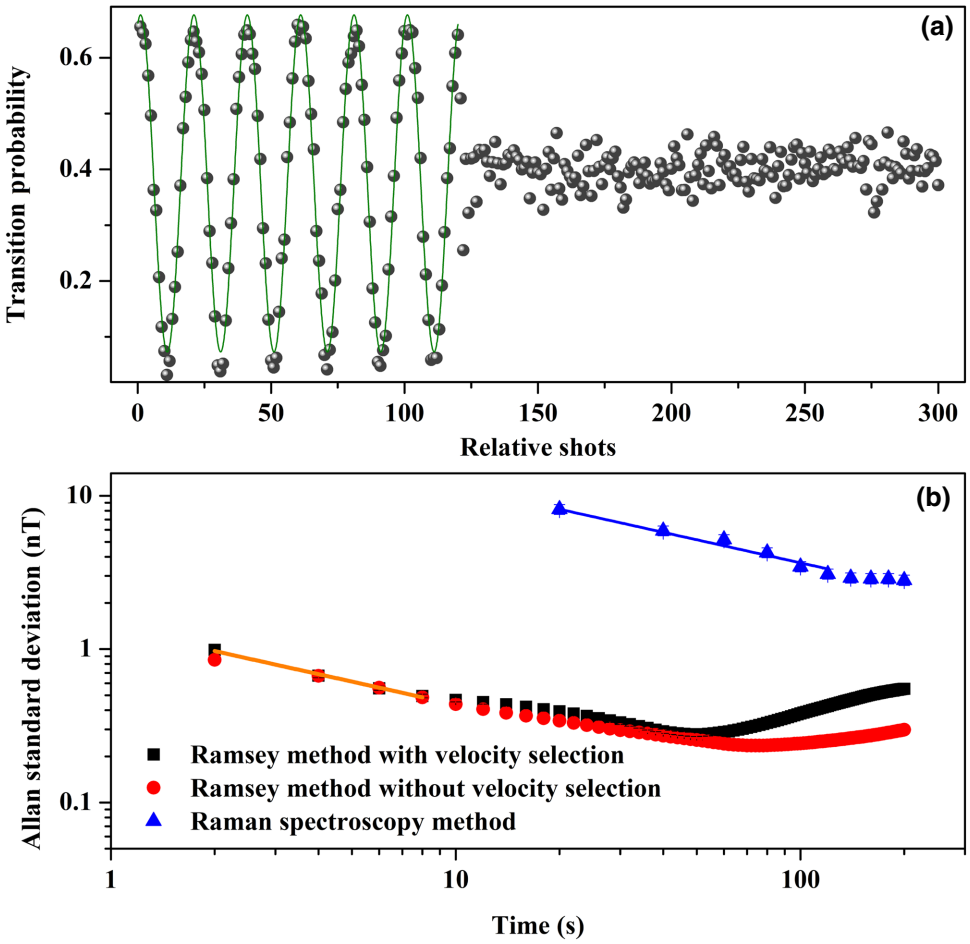

FIG. 6. (a) Demonstration of the switch between full-fringe scanning mode and fringe-locking mode. (b) Allan standard deviations of the magnetic field measurement. Atoms are prepared in $|m_F = -1\rangle$. The black squares and red dots represent the measurements with and without velocity selection, respectively. The blue triangles correspond to the measurement with the Raman spectroscopy method. The orange (blue) solid line corresponds to a short-term sensitivity of 1.4 nT/Hz$^{1/2}$ (36.5 nT/Hz$^{1/2}$).

density of the atoms within the cloud, and the calculated results are shown in Fig. 5(a). The simulated TOF signals agree well with the experimentally detected TOF signals, which verifies that the multiple peaks are indeed induced by the large spread of the atomic cloud. And it also indicates that velocity selection is effective for improving the spatial resolution.

D. Short-term sensitivity

In order to evaluate the short-term sensitivity for our optical Ramsey interferometer with velocity selection, a continuous measurement is performed. A fringe-locking method is also adopted to improve the sampling rate and sensitivity [49,50]. The switch between full-fringe scanning mode and fringe-locking mode is accomplished automatically by the controlling program, as shown in Fig. 6(a). One measurement of the magnetic field is obtained from every two shots, and according to the acquired long-time data, the Allan deviation can be evaluated, as shown in Fig. 6(b). The sensitivities for Raman spectroscopy and the Ramsey method without velocity selection are also shown in Fig. 6(b). For the sensitivity test, the measurements are all performed around 437 mm using only one magnetic sublevel for the three methods, i.e., $|m_F = -1\rangle$. According to the Allan deviations, the short-term sensitivities for the Ramsey method with and without velocity selection are the same, which is 1.4 nT/Hz$^{1/2}$. The sensitivity for Raman spectroscopy is 36.5 nT/Hz$^{1/2}$. Thus the sensitivity for the Ramsey method is better than that for Raman spectroscopy by a factor of over 20 because of its much longer interrogation time and higher sampling rate. The sensitivity for the Ramsey method here is most likely to be limited by the fluctuation of the atomic fountain and the detection noise. Note that the state preparation with velocity selection induces additional fluctuation of the atomic fountain, which accounts for the deterioration of the long-term Allan deviation in the Ramsey method with velocity selection.

IV. CONCLUSION

In conclusion, we have performed an absolute magnetic field measurement using a Ramsey interferometer based on stimulated Raman transition. Compared with the usual Raman spectroscopy method, the Ramsey method can ensure high precision, and the influence of the ac Stark shift can be largely suppressed. It is also convenient to map the magnetic field along the interference region by Raman stimulation instead of microwave stimulation in an atomic

clock. A Doppler-sensitive state selection is explored for the Ramsey interferometer, which improves both the spatial resolution and fringe contrast. The method presented here is applicable for evaluating the magnetic field effect in precision measurements by atom interferometry.

ACKNOWLEDGMENTS

We thank Professor Min-Kang Zhou and Dr. Qin Luo for valuable discussions. The work is supported by the National Natural Science Foundation of China (Grants No. 11727809, No. 11625417, No. 11904114, and No. 11574099).

[1] A. Peters, K. Y. Chung, and S. Chu, High-precision gravity measurements using atom interferometry, Metrologia **38**, 25 (2001).

[2] Z.-K. Hu, B.-L. Sun, X.-C. Duan, M.-K. Zhou, L.-L. Chen, S. Zhan, Q.-Z. Zhang, and J. Luo, Demonstration of an ultrahigh-sensitivity atom-interferometry absolute gravimeter, Phys. Rev. A **88**, 043610 (2013).

[3] P. Gillot, O. Francis, A. Landragin, F. P. Dos Santos, and S. Merlet, Stability comparison of two absolute gravimeters: Optical versus atomic interferometers, Metrologia **51**, L15 (2014).

[4] C. Freier, M. Hauth, V. Schkolnik, B. Leykauf, M. Schilling, H. Wziontek, H.-G. Scherneck, J. Müller, and A. Peters, in *Journal of Physics: Conference Series* (IOP Publishing, 2016), Vol. 723, p. 012050.

[5] D. Savoie, M. Altorio, B. Fang, L. Sidorenkov, R. Geiger, and A. Landragin, Interleaved atom interferometry for high-sensitivity inertial measurements, Sci. Adv. **4**, eaau7948 (2018).

[6] W.-J. Xu, L. Cheng, J. Liu, C. Zhang, K. Zhang, Y. Cheng, Z. Gao, L.-S. Cao, X.-C. Duan, and M.-K. Zhou *et al.*, Effects of wave-front tilt and air density fluctuations in a sensitive atom interferometry gyroscope, Opt. Express **28**, 12189 (2020).

[7] M. A. Kasevich, E. Riis, S. Chu, and R. G. DeVoe, Rf Spectroscopy in an Atomic Fountain, Phys. Rev. Lett. **63**, 612 (1989).

[8] R. Wynands and S. Weyers, Atomic fountain clocks, Metrologia **42**, S64 (2005).

[9] M. Amaral, L. V. G. Tarelho, M. De Souza, A. C. Baratto, G. d. A. Garcia, S. Muller, J. De Martin Jr, A. Rodriguez, A. Bebeachibuli, and D. V. Magalhães, in *Journal of Physics: Conference Series* (IOP Publishing, 2016), Vol. 733, p. 012020.

[10] G. Rosi, F. Sorrentino, L. Cacciapuoti, M. Prevedelli, and G. Tino, Precision measurement of the newtonian gravitational constant using cold atoms, Nature **510**, 518 (2014).

[11] R. Bouchendira, P. Cladé, S. Guellati-Khélifa, F. Nez, and F. Biraben, New Determination of the Fine Structure Constant and Test of the Quantum Electrodynamics, Phys. Rev. Lett. **106**, 080801 (2011).

[12] S. Fray, C. A. Diez, T. W. Hänsch, and M. Weitz, Atomic Interferometer with Amplitude Gratings of Light and its Applications to Atom Based Tests of the Equivalence Principle, Phys. Rev. Lett. **93**, 240404 (2004).

[13] A. Bonnin, N. Zahzam, Y. Bidel, and A. Bresson, Simultaneous dual-species matter-wave accelerometer, Phys. Rev. A **88**, 043615 (2013).

[14] D. Schlippert, J. Hartwig, H. Albers, L. L. Richardson, C. Schubert, A. Roura, W. P. Schleich, W. Ertmer, and E. M. Rasel, Quantum Test of the Universality of Free Fall, Phys. Rev. Lett. **112**, 203002 (2014).

[15] L. Zhou, S. Long, B. Tang, X. Chen, F. Gao, W. Peng, W. Duan, J. Zhong, Z. Xiong, and J. Wang *et al.*, Test of Equivalence Principle at 1 0- 8 Level by a Dual-Species Double-Diffraction Raman Atom Interferometer, Phys. Rev. Lett. **115**, 013004 (2015).

[16] X.-C. Duan, X.-B. Deng, M.-K. Zhou, K. Zhang, W.-J. Xu, F. Xiong, Y.-Y. Xu, C.-G. Shao, J. Luo, and Z.-K. Hu, Test of the Universality of Free Fall with Atoms in Different Spin Orientations, Phys. Rev. Lett. **117**, 023001 (2016).

[17] P. Asenbaum, C. Overstreet, M. Kim, J. Curti, and M. A. Kasevich, Atom-Interferometric Test of the Equivalence Principle at the 10- 12 Level, Phys. Rev. Lett. **125**, 191101 (2020).

[18] P. Wolf, P. Lemonde, A. Lambrecht, S. Bize, A. Landragin, and A. Clairon, From optical lattice clocks to the measurement of forces in the casimir regime, Phys. Rev. A **75**, 063608 (2007).

[19] V. V. Ivanov, Study of surface potentials using resonant tunnelling of cold atoms in optical lattices, J. Phys. B: At. Mol. Opt. Phys. **45**, 205004 (2012).

[20] X. Alauze, A. Bonnin, C. Solaro, and F. P. Dos Santos, A trapped ultracold atom force sensor with a μ m-scale spatial resolution, New J. Phys. **20**, 083014 (2018).

[21] Q.-Q. Hu, C. Freier, B. Leykauf, V. Schkolnik, J. Yang, M. Krutzik, and A. Peters, Mapping the absolute magnetic field and evaluating the quadratic zeeman-effect-induced systematic error in an atom interferometer gravimeter, Phys. Rev. A **96**, 033414 (2017).

[22] M. Pannetier, C. Fermon, G. Le Goff, J. Simola, and E. Kerr, Femtotesla magnetic field measurement with magnetoresistive sensors, Science **304**, 1648 (2004).

[23] H. B. Dang, A. C. Maloof, and M. V. Romalis, Ultrahigh sensitivity magnetic field and magnetization measurements with an atomic magnetometer, Appl. Phys. Lett. **97**, 151110 (2010).

[24] W. Chalupczak, R. M. Godun, S. Pustelny, and W. Gawlik, Room temperature femtotesla radio-frequency atomic magnetometer, Appl. Phys. Lett. **100**, 242401 (2012).

[25] D. Budker, D. F. Kimball, S. M. Rochester, V. V. Yashchuk, and M. Zolotorev, Sensitive magnetometry based on nonlinear magneto-optical rotation, Phys. Rev. A **62**, 043403 (2000).

[26] Y. Hu, Y. Feng, C. Xu, H. B. Xue, and L. Sun, Loop-locked coherent population trapping magnetometer based on a fiber electro-optic modulator, Appl. Opt. **53**, 2158 (2014).

[27] N. F. Ramsey, A molecular beam resonance method with separated oscillating fields, Phys. Rev. **78**, 695 (1950).

[28] A. D. Ludlow, M. M. Boyd, J. Ye, E. Peik, and P. O. Schmidt, Optical atomic clocks, Rev. Mod. Phys. **87**, 637 (2015).

[29] S. Yanagimachi, K. Mizobuchi, and A. Morinaga, Ramsey-bordé atom interferometer having two arms with different zeeman sublevels, Phys. Rev. A **64**, 041601 (2001).

[30] A. A. Wood, L. M. Bennie, A. Duong, M. Jasperse, L. D. Turner, and R. P. Anderson, Magnetic tensor gradiometry using ramsey interferometry of spinor condensates, Phys. Rev. A **92**, 053604 (2015).
[31] V. Gerginov, N. Nemitz, S. Weyers, R. Schröder, D. Griebsch, and R. Wynands, Uncertainty evaluation of the caesium fountain clock ptb-csf2, Metrologia **47**, 65 (2009).
[32] G. D. Domenico, L. Devenoges, A. Stefanov, A. Joyet, and P. Thomann, Fourier analysis of ramsey fringes observed in a continuous atomic fountain for in situ magnetometry, Eur. Phys. J. Appl. Phys. **56**, 11001 (2011).
[33] D. Braje, S. Desavage, C. L. Adler, J. P. Davis, and F. A. Narducci, A frequency selective atom interferometer magnetometer, J. Mod. Opt. **61**, 61 (2014).
[34] F. Fang, M. Li, P. Lin, W. Chen, N. Liu, Y. Lin, P. Wang, K. Liu, R. Suo, and T. Li, Nim5 cs fountain clock and its evaluation, Metrologia **52**, 454 (2015).
[35] Y. Ovchinnikov and G. Marra, Accurate rubidium atomic fountain frequency standard, Metrologia **48**, 87 (2011).
[36] Q. Wang, N. Zhang, W. Guang, S. Zhang, W. Wang, R. Wei, and Y. Wang, Precision measurements of the ground-state hyperfine splitting of rb 85 using an atomic fountain clock, Phys. Rev. A **100**, 022510 (2019).
[37] J. R. Maze, P. L. Stanwix, J. S. Hodges, S. Hong, J. M. Taylor, P. Cappellaro, L. Jiang, M. V. G. Dutt, E. Togan, and A. S. Zibrov *et al.*, Nanoscale magnetic sensing with an individual electronic spin in diamond, Nature **455**, 644 (2008).
[38] S. Beattie, B. Jian, J. Alcock, M. Gertsvolf, R. Hendricks, K. Szymaniec, and K. Gibble, First accuracy evaluation of the nrc-fcs2 primary frequency standard, Metrologia **57**, 035010 (2020).
[39] Q. Wang, N. Zhang, W. Zhao, Q. Ji, R. Dong, R. Wei, and Y. Wang, Evaluation of the radial inhomogeneity of a magnetic field by magnetic-sensitive ramsey interference fringes at 87 rb atomic fountain clock, JOSA B **37**, 1775 (2020).
[40] Z. Zhou, R. Wei, C. Shi, T. Li, and Y. Wang, Magnetic field measurement based on a stimulated two-photon raman transition, Chin. Phys. B **20**, 034206 (2011).
[41] A. Srinivasan, M. Zimmermann, M. A. Efremov, J. P. Davis, and F. A. Narducci, Measurement of magnetic field gradients using raman spectroscopy in a fountain, Proc. SPIE **10119**, 101190Z (2017).
[42] B. Wu, Z. Wang, B. Cheng, Q. Y. Wang, A. P. Xu, and Q. Lin, Accurate measurement of the quadratic zeeman coefficient of 87rb clock transition based on the ramsey atom interferometer, J. Phys. B **47**, 015001 (2013).
[43] S. R. Jefferts, J. H. Shirley, T. E. Parker, T. P. Heavner, D. M. Meekhof, C. Nelson, F. Levi, G. A. Costanzo, A. De Marchi, and R. E. Drullinger *et al.*, Accuracy evaluation of nist-f1, Metrologia **39**, 321 (2002).
[44] Q.-Q. Hu, C. Freier, Y. Sun, B. Leykauf, V. Schkolnik, J. Yang, M. Krutzik, and A. Peters, Observation of vector and tensor light shifts in rb 87 using near-resonant, stimulated raman spectroscopy, Phys. Rev. A **97**, 013424 (2018).
[45] D. A. Steck, Rubidium 87 d line data (2010).
[46] M.-K. Zhou, L.-L. Chen, Q. Luo, K. Zhang, X.-C. Duan, and Z.-K. Hu, Effect of the gaussian distribution of both atomic cloud and laser intensity in an atom gravimeter, Phys. Rev. A **93**, 053615 (2016).
[47] Y.-y. Xu, J.-f. Cui, K. Qi, X.-b. Deng, M.-k. Zhou, X.-c. Duan, and Z.-k. Hu, On-site calibration of the raman laser absolute frequency for atom gravimeters, Phys. Rev. A **97**, 063626 (2018).
[48] J. Cui, Y. Xu, L. Chen, K. Qi, M. Zhou, X. Duan, and Z. Hu, Time base evaluation for atom gravimeters, Rev. Sci. Instrum. **89**, 083104 (2018).
[49] X.-C. Duan, M.-K. Zhou, D.-K. Mao, H.-B. Yao, X.-B. Deng, J. Luo, and Z.-K. Hu, Operating an atom-interferometry-based gravity gradiometer by the dual-fringe-locking method, Phys. Rev. A **90**, 023617 (2014).
[50] X.-B. Deng, X.-C. Duan, D.-K. Mao, M.-K. Zhou, C.-G. Shao, and Z.-K. Hu, Common-mode noise rejection using fringe-locking method in wep test by simultaneous dual-species atom interferometers, Chin. Phys. B **26**, 043702 (2017).